Robotic Tracking and Marking of Surface Shape Defects on Moving Automotive Panels

Valentin Borsu and Pierre Payeur

School of Information Technology and Engineering
University of Ottawa
Ottawa, ON, Canada
[vbors100, ppayeur]@uOttawa.ca

Abstract—**This paper examines the complex problem of robotic interaction with moving panels exhibiting few distinctive visual features, in the context of marking surface deformation defects for quality control in the automotive industry. In order to integrate a defects detection station and a robotic tracking and marking system within a unified framework, an original inter-calibration technique is developed, which allows for the distribution of these systems in two different stations along the assembly line. A robotic prototype for performing the marking operation on a moving panel, using a spraying gun, is built and its operation validated under realistic industrial scenarios. The marking accuracy that is achieved demonstrates the suitability of the proposed robotic solution to perform fully automated region marking of deformations over large surfaces and for substantial volumes of production, while relying only on passive stereoscopy.**

Keywords- stereoscopic vision; calibration; visual servoing; motion prediction.

I. Introduction

Quality control in the automotive industry is essential in order to ensure that the products meet specific standards. Identifying deformation defects, such as dings and dents over the surface of body panels, and fixing them before the panels are assembled on a vehicle is crucial. In current industrial settings, the identification of small deformations usually requires a lengthy manual surface rubbing operation during which the deformations are marked by workers. The proposed research aims at automating this process with the use of vision sensors and a manipulator robot.

For the robot to perform defects marking operations on a moving part, vision and range sensors must provide accurate and real-time data regarding the pose and motion of the panel. Additionally, precise inter-calibration procedures are needed to properly integrate the data provided by the defects detection stage with the pose and motion estimations used to guide the robotic marking operation. Le and Ng [1] investigated the calibration of multiple sensing devices in a large system and proposed an approach relying on maximum likelihood estimation in order to calibrate at once a manipulator robot, a stereoscopic sensor and a laser projector. However, one of the requirements of this technique, which makes use of checkerboards and planar

surfaces, is that all subsystems must coexist within the same location. A more general framework therefore needs to be developed for the 3D vision-based defects detection and robotic marking stations to be distributed along the assembly line, to better accommodate space constraints and for improved pipeline scheduling and production rates.

Kak *et al.* [2, 3] and Chang *et al.* [4] identified the limitations that impeded existing approaches, developed for robotic interaction with moving objects [2, 3, 5], from being turned into commercial products. While the lack of robust and objective methods to evaluate the empirical performance remains an issue, the difficulty of tracking industrial panels, which often suffer from a lack of distinctive features over their surfaces is even more challenging [2]. As a result, the most popular feature extraction and tracking algorithms [6, 7] still experience important limitations [8, 9] when dealing with weakly textured surfaces, as exemplified with unfinished automotive panels at the stage of inspection.

Apart from the general appearance of the automotive panels, the pose and motion estimator (PME) needs to be robust to the complexity of industrial settings. Specifically, the vision-based PME needs to keep track of the moving target panel even though the manipulator robot moves within its field of view, while marking the deformations. Also, the sporadic appearance of factory associates in the view of the vision sensors must not compromise the visual servoing data sent to the robotic arm for the solution to be adequate for industrial assembly processes.

While the detection of tiny deformations over the panels [10] is beyond the scope of this work, the paper has a dual objective. Extending the initial integration between a vision-based defects detection stage and the robotic tracking and marking station [9], this paper introduces an innovative inter-calibration technique between the two stages. The latter is executed on-line, supports the physical separation of the two stations, and does not require a calibration target. The development of a robotic defects marking system over moving panels, relying on passive stereoscopy, is also detailed and experimentally validated.

II. Experimental Vision-Robotic Platform

The complete framework designed for the surface deformation defects detection and marking is shown in Fig. 1, where the functional block for the robotic tracking and

marking station is highlighted in gray. The other major block of this integrated solution is responsible for automatically detecting 3D surface defects [10]. A 3D imaging module for data acquisition, which consists of a structured light sensor (SLS) generates a dense colored 3D reconstruction of the surface profile of the panel under inspection. The 3D surface model is analyzed by the surface deformations detection system which extracts 3D features at various resolutions, groups and classifies them. Finally, the 3D locations of the surface deformations, expressed with respect to the left camera of the SLS sensor, $CamL_{SL}$, are encoded to drive the robotic marking system toward the points where a washable paint must be sprayed. A complete view of the integrated surface deformations detection and marking system is presented in Fig. 2.
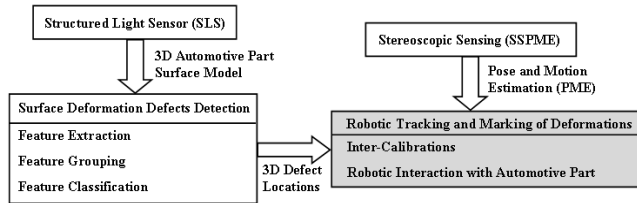

Figure 1. Deformations detection and robotic marking framework.

In this configuration, the SLS is integrated in the same work cell as the stereo-vision sensor used for the pose and motion estimation (SSPME) of the automotive panel. However, the proposed integration permits the transition to a dual station implementation where the marking operation can be performed at a subsequent stage along the assembly line, after the defects detection procedure. Such a separated structure also offers the advantage of permitting the deformations detection system to process data about the following panel while the marking is executed over a previously inspected panel. The SSPME relies on two Point Grey Flea2 IEEE-1394b CCD cameras with 8.5mm lenses and 640x480 pixels of resolution. A 44.5cm baseline is used between the cameras, as it provides improved accuracy in reconstructing the sparse structure of the panel. The automotive part is located at approximately 310cm from the acquisition system. The assembly line consists of a 54cm sled system driven by a separate motor at variable speeds, and the actual interaction with the automotive panel is performed by an F3 7DOF CRS manipulator.
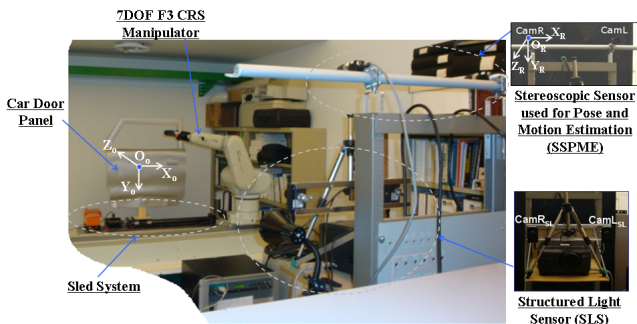

Figure 2. Experimental integrated vision-robotic platform for deformations detection and marking.

As shown in Fig. 1, the robotic marking system relies on the PME of the panel and performs the path planning to guide the marking operation of all detected deformations. The developed PME embeds a supervisory layer [8] whose objective is to provide accurate, time-efficient and fault-tolerant visual servoing data to the robotic station. The only knowledge provided to the supervisory layer is related to a limited number of macro-features (MFs), which are pre-selected over the structure of the automotive panels by the installation engineer when configuring the robotic tracking and marking station. These MFs are shown in Fig. 3a and 3b for two typical rigid panels used in the experimentation, respectively a car door and a fender. The MFs are pre-selected only once and the PME has the internal ability to autonomously re-initialize the set of MFs as soon as a new automotive panel of the same type enters the view of the SSPME for the defects marking operation.

The developed PME embeds classical feature extraction and tracking algorithms [6, 7]. The well-known limitations of these approaches when applied on weakly textured automotive panels moving in a complex environment [8] are addressed from a software perspective, without complicating the passive vision sensing architecture. In order to guarantee consistent movements between the inspected panel and the robot end-effector, two inter-calibration procedures need to be performed. The first one involves the computation of the rigid transformation between the SSPME, whose reference frame is assigned to the right camera, CamR, and the robotic base, whose reference frame O_B, is shown in Fig. 4a. The second inter-calibration relates CamR with the reference frame of the SLS, $CamL_{SL}$, and provides the extra capability to physically separate the defects detection and robot marking systems in two different and successive stations.
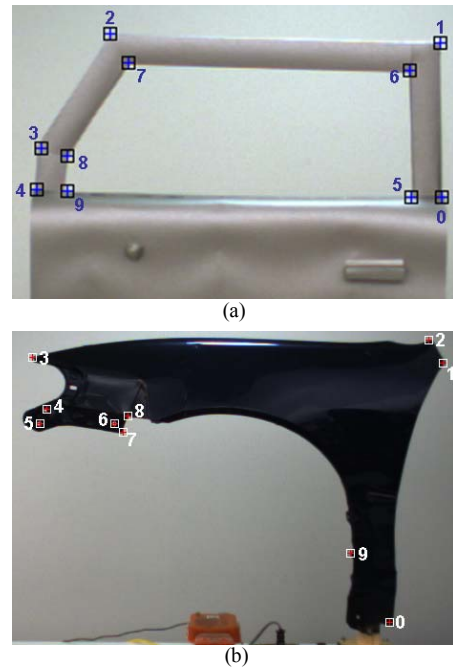

(a)

(b)

Figure 3. Initally selected MFs over the surface of: (a) a car door, (b) a fender.

Different tools were mounted on the robot at various phases of testing, as seen in Fig. 4b and 4c. The first end-effector, shown in Fig. 4b, is a compliant stamping tool that was used to mark the defects by contacts over the automotive panels. It uses a spring-loaded plate as its tip, which allows a compliant deflection of about 1.5cm. For the second alternative, aiming at reproducing in the laboratory the on-line defects marking process that would be performed by a spraying gun, an LED pointing tool, shown in Fig. 4c, was designed. This LED pointer highlights the deformation area and allows for a visual estimation of the accuracy of the marking process while avoiding the dirt and single time marking of actual paint spraying.

Since the detected deformations require to be repaired by factory associates at a later stage of the assembly process, the on-line robotic marking system does not command for extreme accuracy. The goal is rather to efficiently spot the regions within which the deformations appear. As a result, regions of a few (2-3) centimeters diameter are marked, which must contain the actual deformation locations for the process to be validated. When marked with paint, these regions later on, serve as visual guides for the factory associates who perform the repairs.
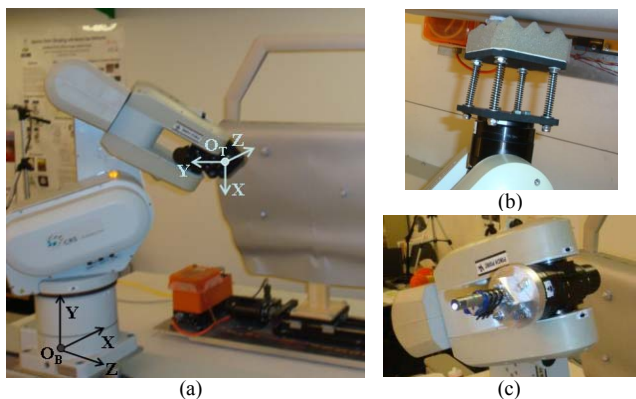

Figure 4. (a) Manipulator robot with different tools: (b) compliant stamp, (c) LED pointer/sprayer

III. SYSTEMS INTEGRATION

For the robot to properly follow the moving panel, an inter-calibration between the SSPME and the robot base is required. It is achieved with the help of a checkerboard pattern that can be attached to the robotic gripper. While the robot is driven to 15 predefined configurations, the checkerboard corners are simultaneously acquired in the reference frames of the robot base and of the SSPME. The resulting sets of 3D coordinates are used to compute the rigid transformation $Q_{CamR/Base}$, using the procedure proposed by Arun *et al.* [11]. An explicit description of this implementation is presented in [9].

A. SLS/SSPME Inter-calibration

For transferring the 3D locations of the defects from the SLS reference frame, where the deformations are identified, to that of the SSPME, which tracks the panel and guides the

robot, a second inter-calibration procedure is performed. In the simplified case where the SLS is installed in the same work cell as the SSPME, the inter-calibration based on the manipulated checkerboard that is described above can be applied.

In order to design a flexible solution that can be adapted to a wide variety of industrial configurations, a calibration technique is proposed for the more general scenario where the deformations detection and the robotic marking stages do not share the same workspace, which preempts the acquisition of the same feature points by the two different vision systems at the same time. Furthermore, the pose of the automotive part with respect to the SLS is likely to exhibit considerable variations when compared to its attitude relative to the SSPME. The differences mainly originate from the 3D surface imager performing the scanning operation from a shorter distance to the object, in order to optimize the accuracy of the model, which is critical for identifying tiny deformations. Conversely, the SSPME is positioned approximately 3m away from the panel in order to maximize the section of the assembly line over which the moving panel appears in both stereo views.

In order to accommodate these constraints, an original solution is proposed that makes use of the few MFs pre-selected over the structure of the automotive parts. The MFs pre-selection and refinement process, performed in the robotic tracking and marking station, is extrapolated to the 3D scanning and deformations detection stage, as the SLS also relies on a higher resolution and calibrated stereoscopic sensor. Under this framework, the installation engineer also selects the location of the MFs, only once, in the left view of the SLS, when configuring the system to inspect a specific type of automotive panels. Then, as the inspection cycle is reiterated on a subsequent panel, the set of MFs is automatically re-initialized [8]. Subsequently, the feature correspondence between the two stereo-views is guided by the pyramidal LK tracker [7], and refined with the Shi and Tomasi corner detector [6]. Based on the computed correspondences and the full calibration of the SLS, a linear triangulation [12] is used to recover the 3D position of the MFs at re-initialization. Nevertheless, the subsequent panels can exhibit slight variations in their pose with respect to the SLS without compromising the detection of the MFs. The refined MFs in the image acquired by $CamL_{SL}$ during the re-initialization procedure for the car door are illustrated in Fig. 5a. Figure 5b shows the MFs refined in the frame acquired by $CamR_{SL}$ and the epipolar lines corresponding to the MFs extracted in $CamL_{SL}$'s frame.

Unlike the inter-calibration performed between the SSPME and the robot base, the inter-calibration between $CamL_{SL}$ and CamR is executed on-line, for every inspected object, once the MFs set is re-initialized in the views of the SSPME, after the completion of the deformations detection cycle for that specific automotive part. The choice of a recurrent inter-calibration is supported by two factors. First, a higher flexibility is provided to the defects detection station, in that the SLS can modify its pose during the inspection phase. Second, the inter-calibration only relies on

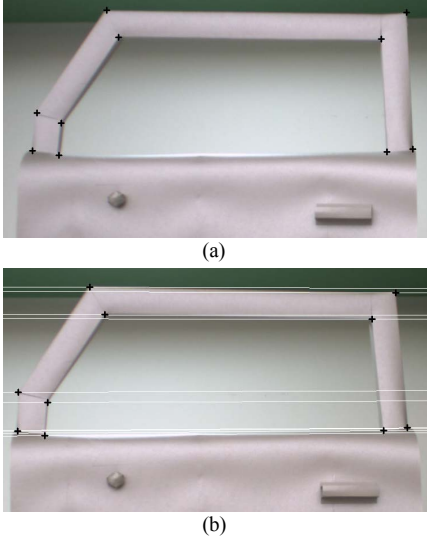a limited number of MFs (N_{MF}=10 in the case of the car door and fender), and takes only a few milliseconds.

(a)

(b)

Figure 5. (a) MFs in CamL$_{SL}$, (b) MFs and their associated epipolar lines in CamR$_{SL}$.

The 3D MFs point cloud reconstructed in the SLS reference frame (CamL$_{SL}$), together with the 3D MFs set recovered at re-initialization with respect to CamR, are used as inputs to the least-squares motion estimation approach proposed by Arun *et al.* [11]. Thus, the transformation matrix $Q_{CamL_{SL}/CamR}$ is computed and the 3D MFs, recovered in the SLS reference frame, are transferred in the SSPME reference frame.

With the purpose of evaluating the performance of the inter-calibration procedure, an analysis of the estimation error is performed on a set of 30 running scenarios involving various attitudes of the two automotive panels, used in the experimentation, with respect to the SLS, and the SSPME, respectively. The proposed analysis examines the maximum of the absolute error, $M_{|\varepsilon|}$, and the RMS error, ε_{RMS}, between the reconstructed and estimated 3D MFs region. The reconstructed MFs, $\overrightarrow{MF_i}^{CamR}$, i=0, $\cdots$,N_{MF}-1, are recovered by employing the linear triangulation technique [12] on the feature correspondences computed in the views of the SSPME [8]. Conversely, a MF defined in CamL$_{SL}$ reference frame, $\overrightarrow{MF_i}^{CamL_{SL}}$, i=0,$\cdots$,$N_{MF}$-1, can be estimated in CamR reference frame, according to the equation:

$$\overrightarrow{\widetilde{MF_{i_{est}}}}^{CamR} = Q_{CamL_{SL}/CamR} \cdot \overrightarrow{\widetilde{MF_i}}^{CamL_{SL}} \qquad (1)$$

in which $\overrightarrow{\widetilde{MF_i}}^{CamL_{SL}}$, $\overrightarrow{\widetilde{MF_{i_{est}}}}^{CamR}$ are expressed in homogenous coordinates. Then, the estimation error, ε, is an N_{MF}-dimensional array of coordinates, whose tri-dimensional elements are given by:

$$\varepsilon_i = \overrightarrow{MF_i}^{CamR} - \overrightarrow{MF_{i_{est}}}^{CamR} . \qquad (2)$$

Then, the maximum and RMS errors are:

$$M_{|\varepsilon|} = \max_{i=0,\cdots,N_{MF}} |\varepsilon_i| \qquad (3)$$

$$\varepsilon_{RMS} = \sqrt{E(\varepsilon^2)} \qquad (4)$$

with $E(\varepsilon^2)$ being the mean value of the squared estimation error vector. Fig. 6 compares the 3D MFs area, reconstructed in CamR reference frame, with the estimated MFs region, computed with (1) at the end of the inter-calibration procedure, under a scenario involving the car door model. Also, Table I shows the results obtained for the two error metrics, $\overline{M}_{|\varepsilon|}$ and $\overline{\varepsilon}_{RMS}$, averaged over the 30 tested scenarios.
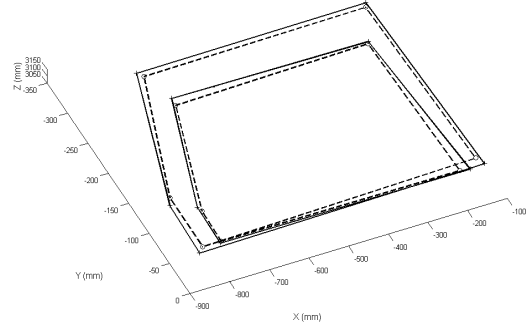

Figure 6. Reconstructed (continuous line)/estimated (discontinuous line) 3D MFs area.

One can observe that the maximum magnitude of the two averaged error measures, computed in the reference frame of CamR, shown in Fig. 2, is obtained along the Z component, followed by a slightly lower error on the X component. The cause of these deviations is three-fold. First, the 3D positions of the MFs are not extremely accurate, as they are affected by the precision of the calibration data, the stereo correspondence and the triangulation process [12]. Second, the considerable difference in the resolution of the cameras used by the SLS (1392x1040 pixels) and that of the SSPME cameras (640x480 pixels) also introduces a drift between the exact location of the MFs within the inner and outer frame of the door's opening. Finally, the procedure used for estimating the rigid transformation, $Q_{CamL_{SL}/CamR}$ builds upon a least-squares approach, thus actively contributing to the error measures shown in Table I.

However, the accuracy provided by the proposed MFs-based inter-calibration is acceptable for the integration of the 3D deformations detection block with the autonomous robotic marking station, as the computed displacement errors in Table I are within 2cm, that is the precision needed for the marking operation. As a result, the developed inter-calibration meets the requirements of the industrial application considered, whose final objective is for the robot to mark the deformation area, and not necessarily its centroid.

The averaged errors reported in Table I could be reduced by means of a higher accuracy calibration apparatus, such as a coordinate measuring machine (CMM), but at the price of

reducing the speed and flexibility of the inspection station and the ease of configuration for non-expert factory engineers.

TABLE I.   ERROR ANALYSIS OF THE SLS/SSPME INTER-CALIBRATION.

Averaged maximum absolute error $\overline{M}_{|\varepsilon|}$ (cm)			Averaged root mean squared error $\overline{\varepsilon}_{RMS}$ (cm)		
$\overline{M}_{|\varepsilon|}^X$	$\overline{M}_{|\varepsilon|}^Y$	$\overline{M}_{|\varepsilon|}^Z$	$\overline{\varepsilon}_{RMS}^X$	$\overline{\varepsilon}_{RMS}^Y$	$\overline{\varepsilon}_{RMS}^Z$
1.63	0.89	2.01	0.86	0.45	1.16

The proposed inter-calibration procedure can also be extended to cases where the 3D scanning over the panels is performed with higher accuracy laser metrology range sensors. The same feature extraction approach can be extrapolated to the corresponding 3D images, and upon the detection of the MFs in 2D image generated from the 3D model, their associated 3D points can be easily detected. As a result, the proposed MFs-based inter-calibration represents a general and viable alternative, which supports both the division of the two components of the inspection station, as well as the selection of different technologies for the 3D scanning of the panel.

B. Robotic Marking Tool's Pose Calculation

The robotic manipulator is directly guided toward the detected locations of the deformations while relying on the two inter-calibration estimations. For the identified defects, which are represented by three dings on the car door model in one of the conducted experiments, as shown in Fig. 7, the 3D contact point with the smallest depth with respect to CamR is extracted.
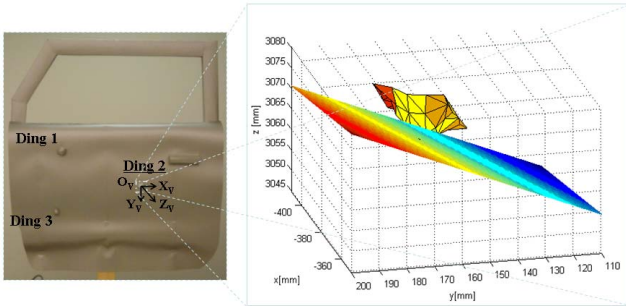

Figure 7.   3D mesh of Ding$_2$ along with the interpolated plane translated on the contact point.

Apart from the location of each detected deformation, the orientation of the marking tool, with respect to the panel's surface in the area that the robot needs to mark, is also estimated. A least-squares interpolation of a plane is computed from the set of all 3D points belonging to the detected deformation, after applying the inter-calibration discussed in Section III.A. The resulting interpolated plane for Ding$_2$, which is translated on the contact point of this defect, is illustrated in Fig. 7. A supplementary reference frame, O_V, is attached to the computed plane, whose origin is defined by the contact point of the deformation area, with the

X_V and Y_V axes parallel to the interpolated plane vectors and the Z_V axis pointing out of the plane, perpendicularly to the local surface patch.

The 3D vectors forming the axes of O_V are normalized to form a rotation matrix which defines the rigid transformation from CamR to the robot's tool, $Q_{Tool/CamR}$. The translation component of $Q_{Tool/CamR}$ is defined by the position of the contact point with respect to CamR. Finally, the transformation defining the pointing pose of the tool with respect to the base of the robot, $Q_{Tool/Base}$, such that the marking operation can be performed, is defined by:

$$Q_{Tool/Base} = Q_{CamR/Base} \cdot Q_{Tool/CamR} . \qquad (5)$$

IV.   EXPERIMENTAL VALIDATION ON MOVING PANELS

This section expands the proposed framework for operation on moving panels and presents the results of the experimental validation of the on-line marking of defects using motion prediction and a paint spraying methodology.

Preliminary tests which preceded the marking operation relying on a spraying gun methodology were conducted with a contact-based marking approach. However, the accuracy of the complete system, originating from the limited resolution of the SLS (which causes a slight bias in the exact location of the defects) [9, 10] and the precision of the PME coupled with the two inter-calibrations, demonstrated the difficulties associated with a contact-based marking strategy, due to variations in the attitude of the tool center point (TCP) with respect to the deformation areas during the motion cycles of the panel [8]. The variations in the depth component of the TCP, programmed to stamp the contact points of the defects, and measured with respect to O_B, had an average magnitude of 2.25cm, which could not be accommodated by the implementation of the spring loaded stamping tool. Such a performance was expectable given that the passive stereoscopic sensor located approximately 3m away from the panel is the only source of information available for the PME. However, the current stereo-vision sensor can be complemented with an additional proximity sensing device that can be mounted on the robotic gripper in order to supervise the close interaction with the moving panel, when performing the contact-based defects marking operation.

On the other hand, the limited ranges over which the depth components vary throughout the motion cycles still support the use of inexpensive passive stereoscopic sensing within an on-line robotic marking architecture that relies on a spraying gun marking methodology. With the latter, the robot does not need to physically touch the moving object since a minimal distance needs to be preserved between the spray gun and the deformation area. This strategy, which appears to be more adequate and fault-tolerant, also satisfies the objective of the proposed robotic application, which is to mark the region that contains the deformation within a few centimeters accuracy, without requiring complex sensing architectures.

A. Robotic Interaction with Motion Prediction

In order to ensure sufficient accuracy for on-line robotic marking, a motion predictor is embedded in the PME. Apart

from the trivial situation where the assembly line is straight and operates at constant speed, the design of the motion prediction system also provides robustness to speed fluctuations and curved sections of the assembly line. The latter result in rotations around the Y_o axis of the panel, as represented in Fig. 2. To provide this level of flexibility, the prediction system builds upon a one-step motion extrapolation methodology. Therefore, the prediction process monitors the rigid transformation characterizing the motion exhibited by the panel between two extracted frames, for instance at time t_i and t_{i+1}, assuming piecewise continuous displacement. This motion estimate is applied on the 3D points corresponding to the detected deformations in order to update their location at time t_{i+1}. This rigid transformation is actually applied twice, in order to also predict the position of the deformation points at time t_{i+2}, when the spraying operation will happen.

The precision of the prediction method was tested with respect to the robotic station, in order to evaluate the effects of the complete PME, coupled with the two inter-calibrations, on the prediction error. For these tests, a scenario in which the sled system was positioned approximately perpendicular to the principal axis of the SSPME was considered. A frame extraction rate of f_{extr}=0.5Hz was set for the PME, and the velocity of the PC-operated sled system fluctuated in the interval [1.2cm/s, 1.6 cm/s]. The total duration of the motion cycle was t_{exp}=36s, whereas the prediction module was triggered after the estimation of the first rigid transformation characterizing the motion exhibited by the panel between the first two subsequent frames. The predicted and estimated locations of $Ding_2$, formed the trajectories shown in Fig. 8a, expressed with respect to O_B. Fig. 8b illustrates the X, Y and Z components of the prediction error, computed as the difference between the estimated and predicted 3D positions of $Ding_2$. As it can be noticed from Fig. 8b, the Y and Z components of the prediction error are inferior to ±2mm, whereas the maximum absolute value of the X components of the displacement error is 9.67mm. This deviation on the predicted depth component can easily be accommodated by the robotic marking system when an LED-pointer or paint spraying gun is used rather than an actual contact-based stamping operation.

Fig. 9 illustrates the block diagram of the on-line robotic operation for spraying deformation defects. Starting from the "home" position, the robot is guided to the pre-contact point of the first defect, which shares the same Y and Z components of the contact point (with respect to O_B), while a reserve of 20cm is extracted from the X component in order to maintain the necessary distance between the spray gun and the surface to be marked. At each frame extraction of the PME, the transformation $Q_{Tool/Base}$, for the current defect, is computed and appended to a data buffer. Once the prediction procedure is triggered, the manipulator robot is driven to the predicted location of the pre-contact point of the first defect. In the situation in which the robot reaches the imposed location before the next frame extraction, it remains in that position in order to perform the spraying operation.
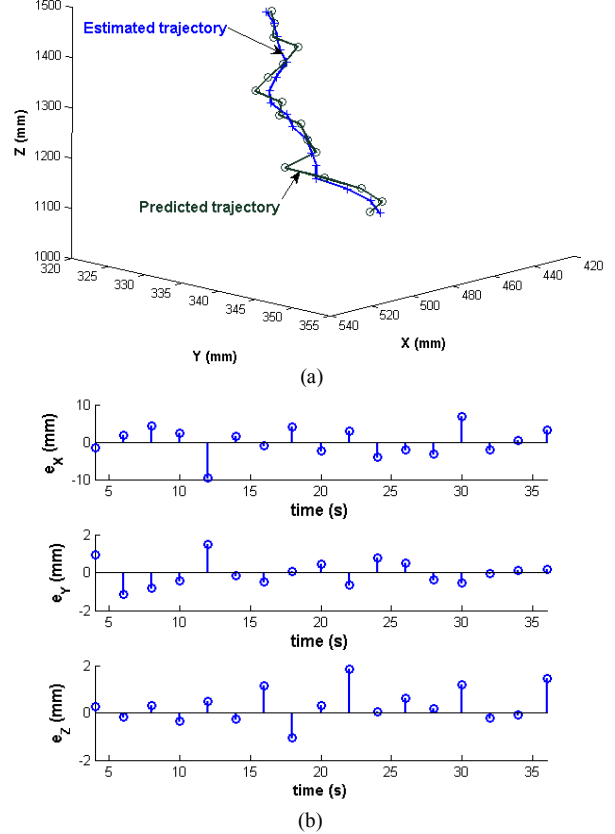

Figure 8. (a) Estimated/predicted trajectory of $Ding_2$, (b) X, Y, Z components of the prediction error.
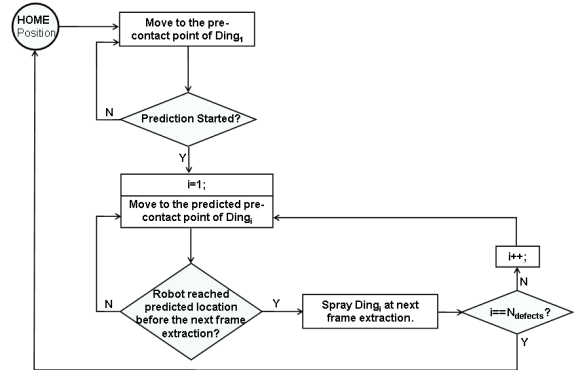

Figure 9. On-line defects spraying operation.

Thus, the triggering of the next frame extraction coincides with the moment at which the spraying occurs, and the index of the defects, i, is incremented. Conversely, if in the interval over which the robot reaches the predicted location, a new set of frames is grabbed by the SSPME, the robot waits for the next prediction data and the same course of action is performed, as illustrated in Fig. 9. This procedure is executed until all the detected deformation defects have been marked. Then, the manipulator robot is driven back to its "home" position and the PME is stopped.

Some samples of images acquired during various testing scenarios, associated with different attitudes of the car door with respect to the SSPME, are shown in Fig. 10. One can see that the projected light falls over the deformation regions in all cases, although the stereo-views are affected by the occlusions caused by the manipulator robot, or the sporadic appearance of a person. Moreover, the results illustrated in Fig. 10c and 10d, which are extracted from two scenarios in which the sled system was slightly rotated around the Y_o axis, as shown in Fig. 2, demonstrate the capability of the proposed solution to handle usual situations where the assembly line contains a curved section, as imposed by space limitation in factory environments. In the circumstances depicted in Fig. 10, with three detected deformations, the total duration of the robotic spraying procedure, as measured from the beginning of the prediction cycle, took $t_{mark\_door}=10s$.

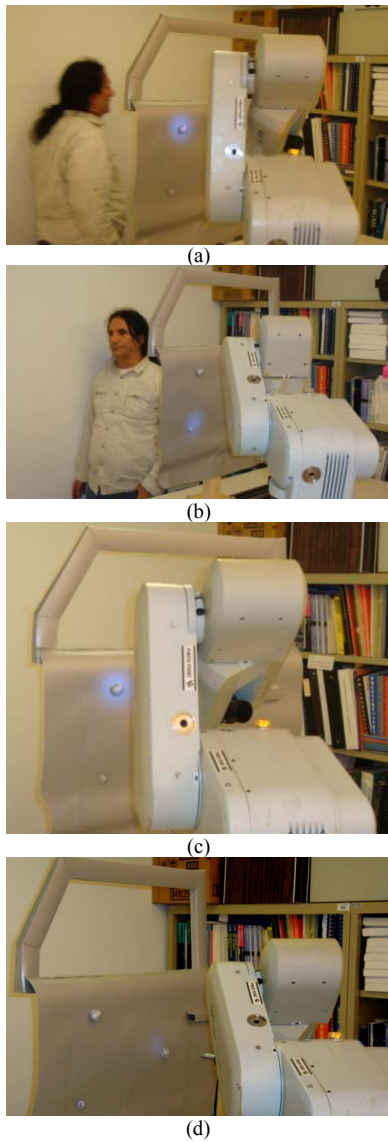In order to validate the generality of the proposed on-line robotic spraying operation, the procedure illustrated in Fig. 9 was also applied on a car fender, shown in Fig. 3b, for which the MFs need to be defined differently from those of the car door. Without loss of generality, the experiments with the fender were only conducted relative to the robotic tracking and marking station. Fig. 11a displays the deformation regions, which were identified from a visual inspection of the fender. Moreover, the relative distances between the locations of these deformations and the closest MF, were measures off-line, according to the reference frame of the SSPME, CamR.
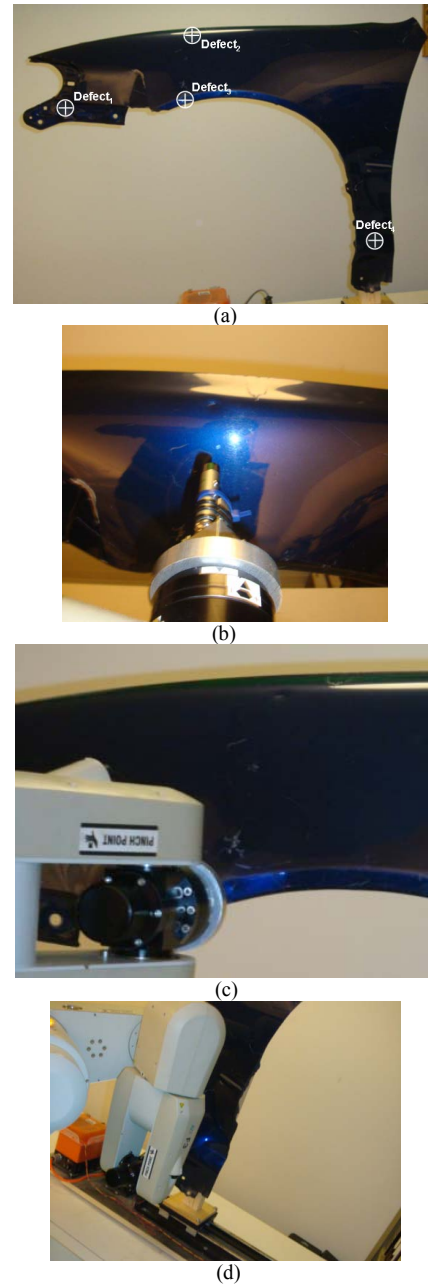

(a)

(b)

(c)

(d)

Figure 10. On-line robotic spraying operation on car door with robot occlusion and personnel movement.

(a)

(b)

(c)

(d)

Figure 11. (a) Detected defects over the fender, and results of the on-line robotic spraying operation on: (b) Defect2, (c) Defect3, (d) Defect4.

Subsequently, during the first 3D reconstruction procedure, performed by the PME, the locations of the corresponding 3D points were determined, using the relative measurements. These 3D points constitute the replica of the data provided by the defects detection station, coupled with the SLS/SSPME inter-calibration. Fig. 11b-d show some samples acquired during the on-line robotic spraying operation, from which, one can see that the projected light falls over the defect regions. In this case, the total marking operation took t_{mark_fender}=15s for four deformations.

The maximum number of deformations that can be marked is inversely proportional to the relative distance between the defects over the surface of the automotive panel. For example, in cases where the defects share a similar relative distance as for the dings on the car door model (i.e. around 30cm), a maximum number of 9 deformation regions can be sprayed, with the current prototype.

Defining the maximum number of defects that can be marked must take into account several factors, such as the field of view of the SSPME, the computational complexity of the PME and the SLS/SSPME inter-calibration, the maximum velocity of the manipulator robot, the distance between the robot's home position and the first defect, and finally, the relative distances between the defects. Therefore, as soon as an upper bound is defined for the maximum number of possibly detectable deformations over a single panel, a trade-off is to be performed between all the above mentioned factors, in order to obtain the most efficient solution.

V. CONCLUSIONS AND FUTURE WORK

This paper described an autonomous robotic system for marking undesired surface deformation defects over moving automotive panels characterized by very few apparent visual features. In order to integrate two separate stations for defects detection and robotic marking within a unified platform, an original inter-calibration technique has been proposed. The latter is performed on-line, supports the duality of the two stations and does not require a calibration target as it uses a low number of structural features already embedded in the inspected object. In order to perform the defects marking operation on moving panels, a robotic prototype relying on a spraying gun end-effector has been designed. Extensive experimental validation demonstrated that satisfactory accuracy and generality can be achieved with this solution, while relying only on visual servoing data provided by passive stereoscopy.

For future work, a more robust kinematic module can be embedded in the motion prediction system. The latter can incorporate a Kalman filter leading to a higher level of generality for the robotic marking station, which will allow for a wider range of motion patterns exhibited by the automotive panel.

REFERENCES

[1] Q. V. Le and A. Y. Ng., "Joint calibration of multiple sensors", Proc. IEEE International Conference on Intelligent Robots and Systems, USA, 2009, pp. 3651-3658, doi:10.1109/IROS.2009.5354272.

[2] Y. Yoon, G. N. DeSouza and A. C. Kak, "Real-time tracking and pose estimation for industrial objects using geometric features", Proc. of the 2003 IEEE Conference on Robotics & Automation, Taiwan, 2003, pp. 3473-3478, doi:10.1109/ROBOT.2003.1242127.

[3] G. N. DeSouza and A. C. Kak, "A subsumptive, hierarchical and distributed vision-based architecture for smart robotics", IEEE. Trans. on Systems, Man and Cybernetics, part B, vol. 34, no. 5, 2004, pp. 1988-2002, doi:10.1109/TSMCB.2004.831768.

[4] T. Chang, T. Hong, M. Shneier, J. Park and R. D. Eastman, "Dynamic 6DOF metrology for evaluating a visual servoing system", Proc. of the 2008 Performance Metrics for Intelligent Systems Workshop, USA, 2008, pp. 173-180, doi:10.1145/1774674.1774702.

[5] L. Davis D. DeMenthon, T. Bestul, S. Ziavras, H. V. Srinivasan, M. Siddalingaiah and D. Harwood, "Robotic acting on moving bodies (RAMBO): Interaction with tumbling objects", Technical Report – Center for Automation Research, University of Maryland, 1989.

[6] J. Shi and C. Tomasi, "Good features to track", Proc. of the 9th IEEE Conference on Computer Vision and Pattern Recognition, USA, 1994, pp. 593-600, doi:10.1109/CVPR.1994.323794.

[7] B. D. Lucas and T. Kanade, "An iterative image registration technique with an application to stereo vision", Proc. of the 1981 DARPA Image Understanding Workshop, 1981, pp. 121-130.

[8] V. Borsu, "Pose and motion estimation of parts exhibiting few visual features for robotic marking of deformations", Masters of Applied Science Thesis, University of Ottawa, Canada, 2010.

[9] V. Borsu, A. Yogeswaran and P. Payeur, "Automated surface deformations detection and marking on automotive body panels", Proc. of the 6th IEEE Conference on Automation Science and Engineering, Canada, 2010, pp. 551-556, doi:10.1109/COASE.2010. 5584643.

[10] A. Yogeswaran and P. Payeur, "Features extraction from point clouds for automated detection of deformations on automotive body panels", Proc. of the IEEE International Workshop on Robotics and Sensors Environments, Italy, 2009, pp. 122-127, doi:10.1109/ROSE.2009. 5355976.

[11] K. S. Arun, T. S. Huang and S. D. Blostein, "Least-squares fitting of two 3-D point sets", IEEE Trans. on Pattern Analysis and Machine Intelligence, vol. 9, no. 5, 1987, pp. 698-700, doi:10.1109/TPAMI. 1987.4767965.

[12] R. Hartley and A. Zisserman, Multiple view geometry in computer vision, Cambridge University Press, UK, 2000.